

# Effects of Micro- and Nano-cellulose on Tensile and Morphological Properties of Montmorillonite Nanoclay Reinforced Poly(lactic Acid) Nanocomposites

Reza Arjmandi, Azman Hassan, M.K. Mohamad Haafiz  
and Zainoha Zakaria

**Abstract** In this chapter, the effects of micro- and nano-cellulose; microcrystalline cellulose (MCC) and cellulose nanowhiskers (CNW), on the properties of montmorillonite (MMT)/poly(lactic acid) (PLA) nanocomposites fabricated using solution casting method were investigated. CNW were isolated from MCC using a chemical swelling method. An initial study showed that the optimum MMT content, based on tensile properties, in PLA/MMT nanocomposite is 5 phr (parts per hundred parts of resin). PLA/MMT/MCC hybrid composites and PLA/MMT/CNW hybrid nanocomposites were produced by incorporating of various contents of MCC and CNW into the optimum formulation of PLA/MMT nanocomposites (P/MT5), respectively. The Young's modulus of PLA/MMT/MCC hybrid composites and PLA/MMT/CNW hybrid nanocomposites increased gradually with increasing MCC and CNW content, respectively. The tensile strength of hybrid composites decreased compared to P/MT5 nanocomposite. However, the tensile strength for the hybrid nanocomposites increased with incorporation of CNW and reached the highest value at 1 phr CNW content. The ductility of hybrid composites and hybrid nanocomposites was also increased significantly from ~10 to ~60 and ~90 % with the incorporation of 1 phr MCC and CNW fillers, respectively. This increase in ductility was proposed to be due to the nucleation of crazes and the formation of shear bands in the PLA. Transmission electron microscopy and X-ray diffraction analyses showed that MCC slightly decreased the MMT interlayer spacing in hybrid composites, while the MMT interlayer spacing in hybrid nanocomposites increased by incorporation of CNW into P/MT5 nanocomposite.

---

R. Arjmandi · A. Hassan (✉)

Department of Bioprocess and Polymer Engineering, Faculty of Chemical and Energy Engineering, Universiti Teknologi Malaysia, 81310 Skudai, Johor Bahru, Malaysia  
e-mail: azmanh@cheme.utm.my

M.K. Mohamad Haafiz

School of Industrial Technology, Universiti Sains Malaysia, 11800 Gelugor, Penang, Malaysia

Z. Zakaria

Faculty of Science, Universiti Teknologi Malaysia, 81310 Skudai, Johor Bahru, Malaysia

**Keywords** Polylactic acid · Montmorillonite · Microcrystalline cellulose · Cellulose nanowhiskers · Hybrid nanocomposites · Tensile properties

## 1 Introduction

In recent years, biodegradable polymers produced from renewable resources have become attractive for practical applications such as medical devices and food packaging (Vroman and Tighzert 2009). Polylactic acid (PLA) is a commercially available biopolymer. It is biodegradable thermoplastic polyester produced from L- and D-lactic acid, which is derived from the fermentation of corn starch (Petersson and Oksman 2006). PLA is a “green polymer” because it can be finally degraded into CO<sub>2</sub> and H<sub>2</sub>O (Liu et al. 2013a). Due to its high strength/stiffness and ease of process, PLA offers a potential alternative to petrochemical plastics in many applications (Huda et al. 2008). However, there are several obstacles for the use of PLA, including low toughness, low impact resistance and moderate gas barrier properties, its inherent brittleness, high production cost and undesirable thermal stability, which are all important properties for packaging applications (Oksman et al. 2006; Sanchez-Garcia and Lagaron 2010). Hence, many approaches have been adopted to overcome these inherent limitations, including the use of plasticizers, polymers blending, layered silicates and other inorganic particles (Sanchez-Garcia and Lagaron 2010; Petersson et al. 2007).

Clay reinforced polymer nanocomposites have received significant attention compared to conventional composites because polymer/clay nanocomposites often exhibit considerable improvement in physical, thermal, mechanical and optical properties and fire retardancy at low filler contents (Hong and Kim 2013). PLA/layered silicate nanocomposites have been shown to exhibit improved tensile strength and Young's modulus compared to neat PLA (Sinha Ray and Okamoto 2003). Montmorillonite (MMT) which consists of two fused silica tetrahedral sheets sandwiching an edge shared octahedral sheet is the most commonly used layered silicate in this respect. However, raw MMT often produces immiscible phases with hydrophobic polymers such as PLA due to its hydrophilic character. For this reason, the ammonium ions are exchanged by more voluminous organic cations, which can strengthen the chemical interaction between PLA and MMT and also induces the formation of layered or exfoliated organic/inorganic nanocomposites (Sinha Ray and Okamoto 2003). MMT reinforced PLA nanocomposites can be prepared by two different methods; namely melt processing and solution casting techniques (Sinha Ray and Okamoto 2003). Based on previous studies, there is no clear optimum content for MMT-based nanocomposites. Thellen et al. (2005) reported that an optimum tensile strength was achieved at a 5 wt% MMT content, while He et al. (2011) and Chang et al. (2003a) showed this occurred at 3 and 4 wt% contents respectively. The Young's modulus has also been shown to increase gradually with an increase in the MMT content. However, these property enhancements are usually accompanied by a severe decrease in ductility. Therefore, there is a need to

investigate ways to produce PLA nanocomposites with both high strength/stiffness and ductility. Besides that, to keep PLA nanocomposites as green as possible and minimize production costs, the addition of renewable, biodegradable and low price reinforcements such as cellulose could be a promising technique (Shayan et al. 2015).

Cellulose is a naturally abundant material which can enhance the biodegradability, mechanical properties, thermal stability and also reduce the production costs of PLA (Herrera et al. 2015; Wang et al. 2014; Karande et al. 2014). Cellulose can be obtained from several sources including bacteria, algae, marine creatures and plants. However, cotton served the highest percentage of cellulose as compared to other sources (>95 %). According to Satyamurthy et al. (2011), a single cotton fiber is consisting of fibrils with the thickness of 20–30  $\mu\text{m}$  and nanometer scale diameters. Microcrystalline cellulose (MCC) is one of the cellulosic derivatives that could be used as fillers in the polymer matrices which can be produced through a combination of mechanical and chemical processing (Chen et al. 2011a; Iwatake et al. 2008; Lu et al. 2008; Mathew et al. 2005). One of the most important properties that could influence the performance of MCC in various applications is the degree of crystallinity. The crystallinity degree of MCC is depending on several factors including displayed the source of cellulose, and processing variables such as the reaction duration and temperature, the extent mechanical agitation applied to the slurry and the drying condition, where usually ranges 55–80 % (Haafiz et al. 2013; Chuayjuljit et al. 2010).

Cellulose nanofibers have been used as a reinforcing filler to enhance the performance of the polymer matrices (Azizi Samir et al. 2005). In terms of performance they possess high specific strength and modulus, easy processability and a relatively reactive surface. Cellulose nanowhiskers (CNW) have been gaining considerable interest among scientists in the last 10 years as potential nano-reinforcement in a number of various polymers. The tensile properties of PLA nanocomposites have been shown to increase when CNW from grass were used as a reinforcement (Pandey et al. 2009). Additionally, CNW obtained from commercial MCC has been shown to improve the storage modulus of neat PLA (Cho et al. 2013). Petersson et al. (2007) reported that CNW improved the storage modulus of PLA at higher temperatures. A study to compare the effect of MMT and CNW on PLA was reported by Petersson and Oksman (2006). They found that MMT increased both yield strength and tensile modulus, whereas CNW only improved the yield strength. Petersson and Oksman (2006) also reported that PLA/CNW nanocomposites have a higher ductility than PLA/MMT nanocomposites. This formed the basis to enhanced the ductility of PLA nanocomposites by incorporation of hybridized fillers. Hybrid fillers can be promising for a number of applications where high strength/stiffness and ductility are required. limited studies have been conducted on the use of hybrid fillers in PLA polymer. Hong and Kim (2013) showed that the simultaneous use of CNW and nanoclay as nanofillers improved the tensile strength and glass transition temperature of PLA using melt mixing.

In this chapter, the effects of micro size MCC and nano size CNW on the tensile and morphological properties of PLA/MMT/MCC hybrid composites and PLA/MMT/CNW hybrid nanocomposites produced by solution casting have been

investigated. The main reason for incorporation MCC and CNW into PLA/MMT nanocomposites is to enhance the Young's modulus and elongation at break of the nanocomposites which are the main properties for packaging materials.

## 2 Materials and Methods

### 2.1 Materials

PLA pellets (3001D) was supplied from NatureWork<sup>®</sup> LLC, Minnetonka, MN USA with a density and melt flow index of 1.24 g/cm and *ca.* 15 g/10 min (190 °C/2.16 kg), respectively. MMT clay was supplied from Nanocor, Inc., Arlington Heights IL, USA (Nanomer 1.30TC), where it was organically modified with octadecylamine (~30 wt%) and has an average particle size of 16–22 μm. MCC filler (Avicel; PH-101) was purchased from Sigma-Aldrich, Malaysia, which was produced from a cotton linter with average particle size of 50 μm. Other reagents such as chloroform, *N,N*-dimethylacetamide (DMAc) (99 % purity) and lithium chloride (LiCl) (99 % Purity) were supplied from Merck, Malaysia.

### 2.2 Production of CNW Using Chemical Swelling

As described by Pereda et al. (2011) and Arjmandi et al. (2015a), CNW were prepared by swelling MCC and separating to whiskers by a sequence of chemical treatment using DMAc and 0.5 % LiCl solution as swelling agents followed by mechanical treatment using a sonication bath (Branson 2510). 10 wt% was the initial concentration of MCC in DMAc/LiCl. Then, MCC was vigorously stirred by a mechanical stirrer inside a water bath at 70 °C for 12 h in order to swell the particles. Subsequently, the swelled MCC particles were sonicated using the same sonication bath for 3 h over a period of 5 days, where long intervals between each sonication period was performed in order to separate the CNW nanofillers. Finally, the gel-like suspension of CNW were repeatedly washed with distilled water, then refrigerated and designated as CNW.

### 2.3 Production of PLA Film

As described in our recent publications (Arjmandi et al. 2014, 2015a, b), PLA pellets (10 g) were dissolved in chloroform (64 ml) at 60 °C for 2 h with constant stirring using a mechanical stirrer. Subsequently, the dissolved PLA was casted on the glass plates and was left at ambient temperature (48 h) to evaporate the solvent and produce the PLA film with the thickness of approximately 100 μm.

## 2.4 Production of PLA/MMT Nanocomposites Film

10 g of PLA pellets with various content of MMT [1–9 phr (parts per hundred parts of resin)] were mixed in order to produce PLA/MMT nanocomposites, as reported in our recent study (Arjmandi et al. 2015a). 64 ml of chloroform were added to the various mixtures of PLA/MMT and stirred using a mechanical stirrer at 60 °C for 2 h. The PLA/MMT suspensions were then sonicated using the same sonication bath (as described earlier) for 5 min and casted on the glass plates to produce PLA/MMT nanocomposite films with ~100 µm thickness. The nanocomposites with 1–9 phr MMT content were produced and designated as P/MT1, P/MT3, P/MT5, P/MT7 and P/MT9. Table 1 presents the formulation of PLA nanocomposites with various MMT contents.

## 2.5 Production of PLA/MMT/MCC Hybrid Composites Film

10 g of PLA pellets, 5 phr MMT and various contents of MCC (1, 3 5 and 7 phr) were mixed in order to fabricate the PLA/MMT/MCC hybrid composites, as described by Arjmandi et al. (2015b). 64 ml of chloroform were added into various mixtures of PLA/MMT/MCC and then stirred using a mechanical stirrer at 60 °C for 2 h. Subsequently, the PLA/MMT/MCC suspensions were sonicated using the same sonication bath (as described earlier) for 5 min and then casted on the glass plates (as described above) to obtain PLA/MMT/MCC hybrid composite films with ~100 µm thickness. The hybrid nanocomposites with 1–7 phr MCC were

**Table 1** Polylactic acid nanocomposites formulation

Designation	PLA (wt%)	MMT (phr)	MCC (phr)	CNW (phr)
PLA	100	0	0	0
P/MT1	100	1	0	0
P/MT3	100	3	0	0
P/MT5	100	5	0	0
P/MT7	100	7	0	0
P/MT9	100	9	0	0
P/MT5/MC1	100	5	1	0
P/MT5/MC3	100	5	3	0
P/MT5/MC5	100	5	5	0
P/MT5/MC7	100	5	7	0
P/MT5/CW1	100	5	0	1
P/MT5/CW3	100	5	0	3
P/MT5/CW5	100	5	0	5
P/MT5/CW7	100	5	0	7
P/MT5/CW9	100	5	0	9

produced and designated as P/MT5/MC1, P/MT5/MC3, P/MT5/MC5 and P/MT5/MC7, as summarized in Table 1.

## **2.6 Production of PLA/MMT/CNW Hybrid Nanocomposites Film**

10 g of PLA pellets, 5 phr of MMT and various content of CNW (1, 3, 5, 7 and 9 phr) were mixed in order to produce the PLA/MMT/CNW hybrid nanocomposites, as explained in our recent publication (Arjmandi et al. 2015a). The CNW nanofiller used was in water suspension form. Solvent exchange was then carried out via centrifugation using a Universal 32 Hettich centrifuge (Newport Pagnell, England). Water was then exchanged with acetone and acetone exchanged with chloroform. The CNW filler was then sonicated using an ultrasonic bath (Branson 2510) for 5 min to ensure a homogenous dispersion inside the chloroform. The dispersed CNW was then transferred into a reaction flask containing PLA pellets and 5 phr of MMT. Subsequently, 64 ml of chloroform added into the various mixtures of PLA/MMT/CNW and the stirred using mechanical stirrer at 60 °C for 2 h. The dissolved PLA containing MMT/CNW was then sonicated for another 5 min. Finally, the PLA/MMT/CNW suspension was casted on the glass plates to obtain nanocomposite films with ~100 µm thickness. The hybrid nanocomposites with 1–9 phr CNW were produced and designated as P/MT5/CW1, P/MT5/CW3, P/MT5/CW5, P/MT5/CW7 and P/MT5/CW9, as summarized in Table 1.

## **3 Characterization**

### **3.1 Tensile Properties**

Tensile testing was performed using an Instron 4400 Universal Tester to measure the tensile strength at the break point and Young's modulus for each formulation. Rectangular specimens were cut from the obtained film with dimension of  $60 \times 13 \times 0.1 \text{ mm}^3$ . The tensile tests were carried out at ambient temperature (ASTM D882-12). A fixed crosshead rate and gauge length of  $12.5 \text{ mm min}^{-1}$  and 30 mm were utilized for all formulations, respectively, and the reported results are the average of 10 samples.

### **3.2 Fourier Transform Infrared Spectroscopy**

A Perkin Elmer 1600 Infrared spectrometer manufactured by USA was used in order to perform the Fourier transform infrared spectroscopy (FTIR). 1 wt% of KBr

was mixed with the specimens which were made in powder form. Also, neat KBr was used as FTIR spectral reference. FTIR of the specimens were recorded at constant scan and resolution of 32 and 4  $\text{cm}^{-1}$ , respectively, using Nicolet's AVATAR 360 and the wave range of 4000–370  $\text{cm}^{-1}$ . The position of significant transmittance peaks was determined using the “find peak tool” provided by Nicolet OMNIC 5.01 software.

### 3.3 Morphological Properties

Field emission scanning electron microscopy (FESEM) and transmission electron microscopy (TEM) were used in order to characterize the morphologies of specimens. FESEM was carried out using a Carl Zeiss manufactured by Germany (Supra 35 VP microscope) with an accelerating voltage in the range of 8–10 kV. The samples were placed onto specimen stubs and sputter-coated with gold prior observation to prevent from the accumulation of electrostatic charges on the surface of the samples during electron irradiation. Then, the coat samples were then examined in a FESEM. In addition to FESEM, the microstructure of the neat PLA and its hybrid composites and hybrid nanocomposite in order to investigate the fillers dispersion in the PLA matrix were carried out using a TEM, JEOL JEM-2010, USA. The TEM samples were sectioned using an ultra-microtome, RMC (model MTXL) to obtain thick slices ( $\sim 70$  nm). Then the samples were negatively stained by allowing the grids to float in a 1 % uranyl diacetate solution for 3 min. The samples were examined at an accelerating voltage of 120 k. The TEM images were obtained using soft imagine system software.

### 3.4 X-Ray Diffraction

X-ray diffraction (X-RD) analysis was carried out to study the structures of hybrid composites and hybrid nanocomposites using a Siemens D5000 X-ray diffractometer manufactured by Berlin, Germany. The diffraction patterns (Ni-filtered Cu  $K\alpha$  radiation) were recorded using a step size of 0.02°,  $2\theta = 2.0 - 10^\circ$  ( $2\theta$  angle range). The operating voltage and current were 40 kV and 50 mA, respectively. According to Bragg's Law, the interlayer distances (*d-spacing*) of the MMT layers in the hybrid composites and hybrid nanocomposites were obtained from the peak positions in the X-RD patterns and calculated using Eq. (1).

$$d\text{-spacing} = \frac{n\lambda}{2 \sin \theta} \quad (1)$$

where  $n$  is an integer ( $n = 1$ ),  $\theta$  is the diffraction angle and  $\lambda$  is the X-ray wavelength,  $\lambda = 0.15406$  nm (Cu  $K\alpha$ ).

## 4 Results and Discussion

### 4.1 Tensile Properties

Figure 1a–c reports the tensile properties of PLA/MMT nanocomposites, PLA/MMT/MCC hybrid composites and PLA/MMT/CNW hybrid nanocomposites, respectively. Figure 1a presents the tensile strengths and Young's modulus of the PLA and PLA/MMT nanocomposites at various MMT contents (Arjmandi et al. 2015a). The tensile strength of PLA/MMT nanocomposites is observed to increase with the addition of MMT, reaching a plateau at a filler content of 5 phr, then declining at higher contents. The tensile strength of PLA/MMT nanocomposites at a 5 phr filler content is  $\sim 63\%$  higher than that of the neat PLA, suggesting a significant reinforcing effect of the inorganic phase. It is thought that at this filler content the MMT is distributed uniformly within the PLA matrix. As a result, at this filler content, the tensile strength reaches a maximum value. However, when the filler content exceeds 5 phr, the tensile strength dramatically decreases probably due to the aggregation of the filler resulting in stress concentration points for fracture. This result is in agreement with Lee et al. (2008), where the agglomeration

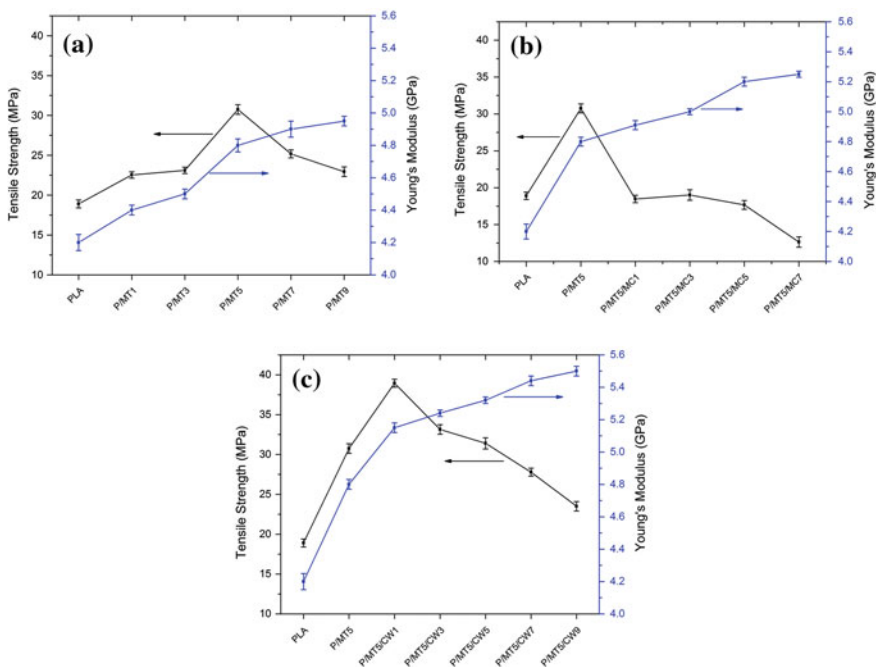


**Fig. 1** Tensile strength and Young's modulus of **a** PLA/MMT nanocomposites, **b** PLA/MMT/MCC hybrid composites and **c** PLA/MMT/CNW hybrid nanocomposites. Errors presented represent standard deviations from the mean ( $n = 10$ ) (Arjmandi et al. 2014, 2015a)



of MMT at high filler contents (>5 wt%) resulted in a decrease in tensile strength. However, the Young's modulus of MMT reinforced PLA nanocomposites increased gradually with increasing MMT content. It is notable that the Young's modulus of nanocomposites at 9 phr MMT content increased by approximately 18 % compared to neat PLA film. This increase is attributed to the rigid MMT fillers which constrict segmental chain motion in the polymer matrix. This result is consistent with a previous reported study by He et al. (2011).

Tensile properties (tensile strength and Young's modulus) of MCC filled PLA/MMT nanocomposites have shown in Fig. 1b, as reported in our recent publication (Arjmandi et al. 2014). As can be observed from Fig. 1b, the Young's modulus of PLA/MMT/MCC hybrid composites increased gradually with increasing MCC content (from 4.8 to 5.31 GPa), where it was higher than PLA/MMT nanocomposites. This improvement in modulus of hybrid composites was likely due to the stiffening effect of the high modulus MCC fillers. Haafiz et al. (2013) were reported similar trend, where MCC filled PLA composites. In contrast, the tensile strength of PLA/MMT/MCC hybrid composites decreased by incorporating of MCC into PLA/MMT nanocomposites, where the tensile strength decreased by ~38 % with incorporation of 1 phr MCC compared to optimum formulation of PLA/MMT nanocomposites (P/MT5). The decrease in tensile strength could be attributed to the aggregation of MCC in PLA hybrid nanocomposites which induced by Van der Waal's forces. From Fig. 1a, b, it is interesting to compare the relative increase in modulus for nanocomposites and hybrid composites. The addition of 7 phr MMT to PLA resulted in a modulus increase to 4.90 GPa, while by addition of MCC (1 phr) to the optimized nanocomposite sample (P/MT5 nanocomposite) produced a slightly higher increase in modulus (4.91 GPa). In addition, it is interesting to note that the Young's modulus of P/MT5/MC3 hybrid composite with the total of 8 phr filler content (5 phr MMT + 3 phr MCC) is higher than the Young's modulus of the P/MT9 nanocomposite with 9 phr MMT content.

On the other hand, Fig. 1c presents the tensile properties (tensile strength and Young's modulus) of CNW reinforced PLA/MMT nanocomposites, as reported in our recent study (Arjmandi et al. 2015a). It was observed that these hybrid nanocomposites (at 1 phr CNW content) had the highest tensile strengths; increases of ~27 and ~106 % were observed compared to those of the P/MT5 nanocomposite and neat PLA, respectively. The highest tensile strength at 1 phr CNW content might be attributed to the homogeneous dispersion and specific interaction that took place between the PLA and both MMT and CNW. This also indicates a positive synergistic effect of MMT and CNW in the enhancement of the tensile strength of the hybrid nanocomposites through the formation of good interactions with the PLA. Similar conclusion has been reported by Wang et al. (2006), where CNW reinforced PLA nanocomposites. When the CNW content was increased beyond 1 phr the tensile strength however decreased. The decrease in tensile strength is thought to be due to the aggregation of MMT platelets induced by Van der Waal's forces and thereby a reduced surface area of interaction between the PLA and both MMT and CNW. This result is in agreement with Liu et al. (2013b) for a halloysite filled PLA polymer. In addition, the Young's modulus of

PLA/MMT/CNW hybrid nanocomposites (Fig. 1c) gradually increased with increasing CNW content (from 4.8 to 5.5 GPa). The Young's modulus of the hybrid nanocomposites increased by  $\sim 23$ ,  $\sim 27$  and  $\sim 31$  % above that of the neat PLA by incorporation of 1, 5 and 9 phr CNW content, respectively. This improvement in Young's modulus could be attributed to the high modulus of both MMT and CNW fillers. Cheng et al. (2009) and Haafiz et al. (2013) were reported similar conclusion, where cellulose fibers and microcrystalline cellulose reinforced PLA composites, respectively.

The elongation at break of PLA/MMT nanocomposites, PLA/MMT/MCC hybrid composites and PLA/MMT/CNW hybrid nanocomposites were summarized in Table 2, as reported in our previous publications (Arjmandi et al. 2015a, b). The hybrid composites and hybrid nanocomposites were observed to have higher ductility compared to MMT reinforced PLA nanocomposites. The elongation at break of PLA/MMT/MCC hybrid composites and PLA/MMT/CNW hybrid nanocomposites significantly increased from  $\sim 10$  to  $\sim 60$  and  $\sim 90$  % by incorporation of 1 phr MCC and CNW into the optimized PLA/MMT nanocomposites (P/MT5), respectively. Petersson and Oksman (2006) reported similar observation, where they found that PLA/CNW nanocomposites have much better ductility compared to PLA/MMT nanocomposites. However, incorporation of higher content of MCC and CNW ( $>1$  phr) decreased the elongation at break of hybrid composites and hybrid nanocomposites significantly. The improvement in ductility of hybrid composites and hybrid nanocomposites is due to the ability of MCC and CNW to restrict the polymer chains' mobility. Due to the aggregation and poor adhesion of MCC in PLA matrix, incorporation of 1 phr MCC filler into P/MT5 nanocomposite decreased the tensile strength of hybrid composites significantly, as discussed earlier. Therefore, it can be concluded that at this filler content (1 phr), aggregation

**Table 2** Elongation at break of (a) PLA/MMT nanocomposites, (b) PLA/MMT/MCC hybrid composites and (c) PLA/MMT/CNW hybrid nanocomposites (Arjmandi et al. 2014, 2015a)

	Designation	Elongation at break (%)
(a)	PLA	124.8 $\pm$ 0.5
	P/MT1	55.0 $\pm$ 0.3
	P/MT3	29.5 $\pm$ 0.5
	P/MT5	10.6 $\pm$ 0.4
	P/MT7	6.4 $\pm$ 0.5
	P/MT9	4.6 $\pm$ 0.3
(b)	P/MT5/MC1	60.1 $\pm$ 0.5
	P/MT5/MC3	35.6 $\pm$ 0.3
	P/MT5/MC5	11.5 $\pm$ 0.4
	P/MT5/MC7	8.6 $\pm$ 0.5
(c)	P/MT5/CW1	89.6 $\pm$ 0.4
	P/MT5/CW3	56.8 $\pm$ 0.3
	P/MT5/CW5	37.7 $\pm$ 0.5
	P/MT5/CW7	33.5 $\pm$ 0.4
	P/MT5/CW9	29.4 $\pm$ 0.3

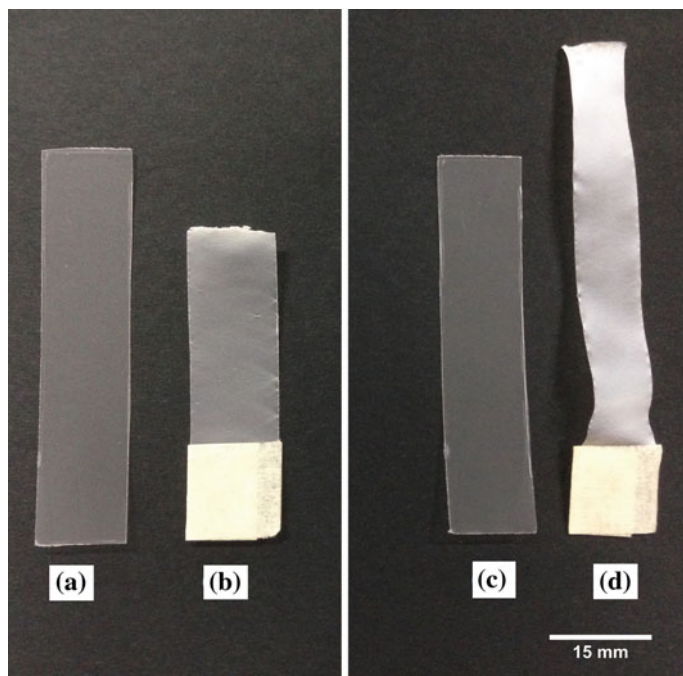
and poor adhesion of MCC is detrimental to tensile strength but not to elongation at break. In contrast, incorporation of 1 phr CNW filler into P/MT5 nanocomposite increased the tensile strength as well because of good dispersion/distribution and adhesion of CNW in PLA matrix, which shows the advantages of nano-size CNW compared to micro-size MCC. Interestingly, although the incorporation of higher content of MCC and CNW (>1 phr) into optimized formulation of PLA/MMT nanocomposites (P/MT5) decreased the elongation at break of hybrid composites and nanocomposites compared to lower content (1 phr), the elongation at break of hybrid composites and hybrid nanocomposites at 3 phr MCC and CNW content was still higher than optimized PLA/MMT nanocomposites. From the current results it can be concluded that the MCC and CNW could play an important role in enhancing the elongation at break of MMT reinforced PLA nanocomposites.

Additionally, increasing ductility seemed likely to be due to their enhanced hydrophilic character as will be confirmed by the FT-IR analysis. Thus, the existence of a proportional content of hydrophilic groups may contribute to plasticization leading to enhanced deformability. It may also be the case that the addition of MCC and CNW leads to nucleation of crazes in the amorphous fraction of the PLA resin, as has been previously observed for a different system (Bulota and Hughes 2012). Typical images of the test specimens of the P/MT5 nanocomposite and P/MT5/CW1 hybrid nanocomposite films before and after deformation (Fig. 2a–d) was reported in our recent study (Arjmandi et al. 2015a). According to Bulota and Hughes (2012), the high strain-to-failure arising from craze nucleation is indicated by a whitening of the polymer matrix due to air scattering. As can be clearly observed from Fig. 2d, P/MT5/CW1 hybrid nanocomposites exhibit much greater ductility compared to P/MT5 nanocomposite, accompanied by pronounced stress whitening. The stress-whitened zone observed in the test specimens suggests the presence of shear bands in the PLA.

Besides that, it is worth noting that the PLA/MMT/CNW hybrid nanocomposites provided higher tensile properties compared to PLA/MMT nanocomposites and PLA/MMT/MCC hybrid composites, as confirmed by typical stress–strain curves in our previous publication (Arjmandi et al. 2015a). Figure 3 presents the typical stress–strain curves of P/MT5 nanocomposite, P/MT5/MC1 hybrid composite and P/MT5/CW1 hybrid nanocomposite. As can be observed from this Fig. 3, the tensile increased compared to P/MT5 nanocomposite and P/MT5/MC1 hybrid composite. An interesting observation from Fig. 3 is that the elongation at break of P/MT5/CW1 hybrid nanocomposite also increased compared to P/MT5/MC1 hybrid composite, which shows the advantages of nano-size CNW compared to micro-size MCC.

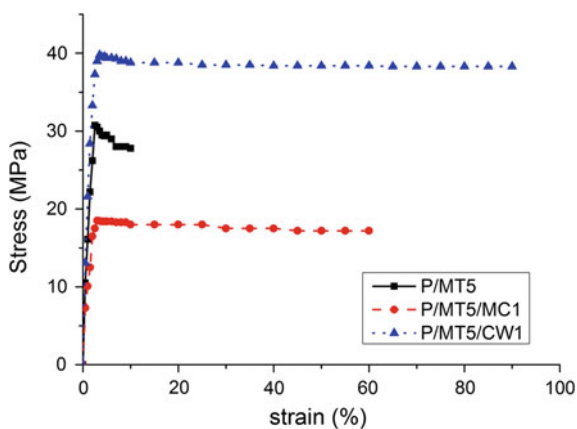
## 4.2 FT-IR Spectroscopy Analysis

Figure 4a–d illustrate typical IR spectra of the neat PLA, P/MT5 nanocomposite, P/MT5/MC1 hybrid composite and P/MT5/CW1 hybrid nanocomposites,



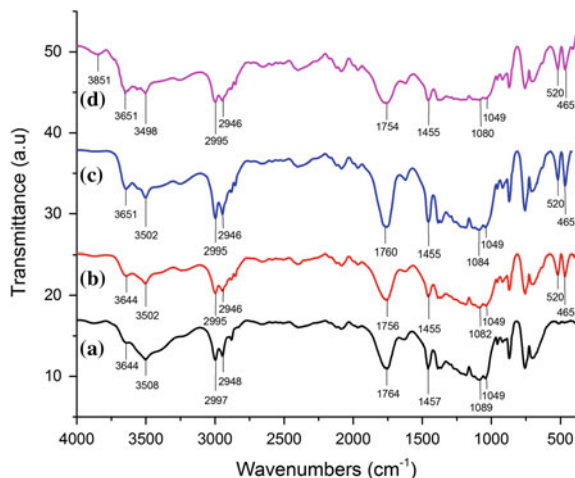
**Fig. 2** Photograph images of the test specimens. **a** P/MT5 nanocomposite film prior deformation, **b** P/MT5 nanocomposite film at  $\sim 10\%$  strain, **c** P/MT5/CW1 hybrid nanocomposite film prior deformation and **d** P/MT5/CW1 hybrid nanocomposite film at  $\sim 90\%$  strain (Arjmandi et al. 2015a)

**Fig. 3** Stress–strain curves of P/MT5 nanocomposite, P/MT5/MC1 hybrid composite and P/MT5/CW1 hybrid nanocomposite (Arjmandi et al. 2015a)



respectively (Arjmandi et al. 2015a, b). As shown in Fig. 4a, the absorption peaks at  $3508$  and  $3644\text{ cm}^{-1}$  attributed to a bending vibration of two terminal hydroxyl groups and the absorption peaks at  $2948$  and  $2997\text{ cm}^{-1}$  are corresponded to an

**Fig. 4** FT-IR spectra of **a** neat PLA, **b** P/MT5 nanocomposite, **c** P/MT5/MC1 hybrid composite and **d** P/MT5/CW1 hybrid nanocomposite (Arjmandi et al. 2015a, b)



asymmetrical stretching vibration of a  $-\text{CH}$  moiety. The absorption peaks at  $1764$  and  $1089\text{ cm}^{-1}$  are assigned to the stretching vibration of  $\text{C}=\text{O}$  groups and stretching vibration of  $\text{C}-\text{O}$  groups, respectively. In addition, the peaks at  $1049$  and  $1457\text{ cm}^{-1}$  attributed to  $-\text{OH}$  and  $-\text{CH}_3$  bending vibrations (Field et al. 2012).

Upon the addition of the MMT into the PLA (Fig. 4b), the absorption peaks at  $1089$ ,  $1764$  and  $3508\text{ cm}^{-1}$  of the PLA shifted to lower wave number positions of ( $1082$ ,  $1756$  and  $3502\text{ cm}^{-1}$ , respectively). Moreover, two new peaks appeared at  $465$  and  $520\text{ cm}^{-1}$  that correspond to stretching vibrations of the  $\text{Si}-\text{O}$  groups of the MMT filler. These changes in the spectra are thought to be due to the good interactions and adhesion between the PLA matrix and the MMT filler which caused by formation of polar interactions between the functional groups of both components (Chen et al. 2011b). It is noticeable that the MMT layers contain huge numbers of polar sites along the structure which distributed uniformly, indicating an electron density content around the surfaces and interlayer spaces. As a result, polar interactions between the MMT filler and PLA matrix thought to readily occur. Liu et al. (2013b) indicated that the shifting of absorption peaks in the IR spectrum of PLA nanocomposites could be due to the formation of hydrogen bonding between the  $\text{Si}-\text{O}$  groups of the MMT and hydroxyl groups of the PLA matrix.

As can be observed from Fig. 4c, the addition of MCC into optimized formulation of PLA/MMT nanocomposites (P/MT5) did not influence the chemical structure of P/MT5 nanocomposite since there is no any new functional group was observed in the IR spectrum of P/MT5/MC1 hybrid composite compared to P/MT5 nanocomposite. This indicates that the MCC fillers did not chemically interact with PLA and only physical interactions occurred between MCC and PLA matrix. Similar observation was reported by Qu et al. (2010). In addition, due to the interactions between the hydroxyl groups of MCC and the carbonyl groups of PLA matrix, the absorption peak at  $3644\text{ cm}^{-1}$  (Fig. 4b) was shifted to higher wavenumber ( $3651\text{ cm}^{-1}$ ) by incorporation of MCC into P/MT5 nanocomposite.

(Fig. 4c). Besides that, the interactions between the  $-OH$  groups of MCC and PLA could have also contributed to this shift.

In contrast, the effect of the addition of CNW on the PLA/MMT nanocomposites is shown in Fig. 4d. A new absorption peak at  $3851\text{ cm}^{-1}$  was observed in the P/MT5/CW1 IR spectrum as compared to the optimized formulation of PLA/MMT nanocomposites (P/MT5). The shift of the peak from  $3644$  to  $3651\text{ cm}^{-1}$  was also observed, which indicating a good interaction between the  $-OH$  groups of the CNW and the  $-OH/C=O$  groups of the PLA. Meanwhile, the presence of a new peak at  $3851\text{ cm}^{-1}$  assigned to a bending vibration of the hydroxyl groups indicating the presence of CNW in the PLA matrix, thereby contributing to the increased hydrophilic character of the hybrid nanocomposites. These findings clearly imply that either the addition of a single filler or the addition of hybrid fillers has changed the molecular conformation of the PLA, thus altering the properties of the nanocomposites.

### 4.3 Optical Microscopy

in our recent study (Arjmandi et al. 2015a), further evidence of crazing and shear banding in the samples was obtained using optical microscopy. The typical light microscope images of the P/MT5/MC1 hybrid composite and P/MT5/CW1 hybrid nanocomposite before and after deformation are presents in Fig. 5a, b, respectively. To better observe the crazes and shear bands, light microscopy images were conducted using back-illumination. Figure 5a, b, clearly shows crazes forming in the sample after deformation (right side images), which look like cracks but characteristically form perpendicular to the draw direction. In addition, the formation of shear bands (at  $45^\circ$  to the direction orthogonal to the tensile axis) were also clearly observed. These shear bands may also increase the toughness of the nanocomposites through localized yielding of the polymer. High strain within a craze zone and the formation of shear bands could result in an overall increase in the strain to failure of the sample.

### 4.4 Field Emission Scanning Electron Microscopy

FESEM micrographs of the fractured cross-sectional surfaces of neat PLA, P/MT5 nanocomposite and P/MT7 nanocomposite are presents in Fig. 6a–c, respectively, as reports in our previous publications (Arjmandi et al. 2015a, b). As can be observed from Fig. 6a, neat PLA has a typical smooth surface (Jiang et al. 2007). Figure 6b reports the fractured cross-sectional surfaces of P/MT5 nanocomposite which shows that the MMT layers are uniformly dispersed in the PLA matrix because of its finer particle size, as indicated by the arrows. Figure 6c reports the fractured cross-sectional surfaces of P/MT7 nanocomposite which clearly shows



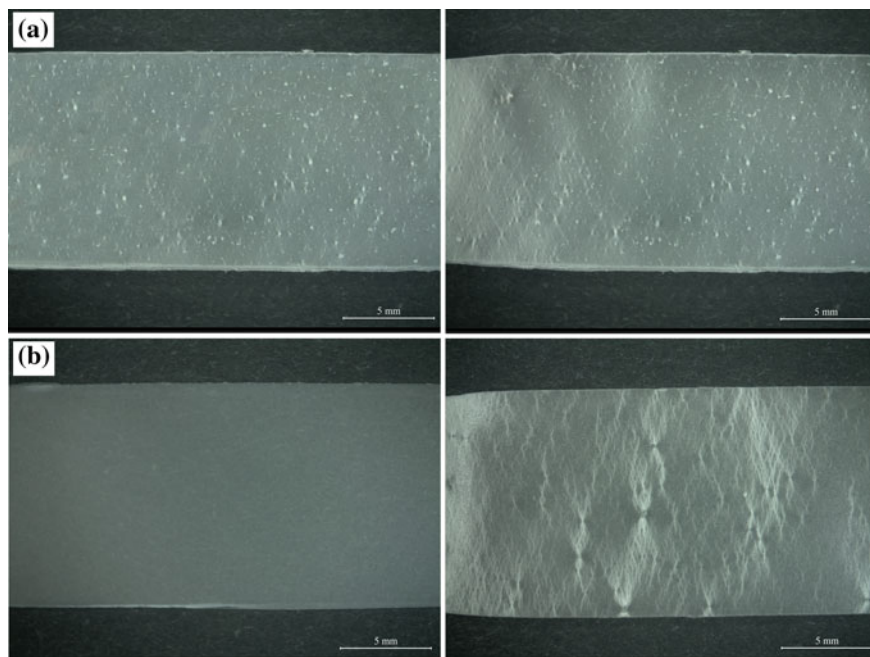


**Fig. 5** Optical microscopy images prior (*left*) and after (*right*) deformation. **a** P/MT5/MC1 hybrid composite film and **b** P/MT5/CW1 hybrid nanocomposite film (Arjmandi et al. 2015a)

that further addition of MMT fillers (>5 phr) can result in MMT aggregation, as indicated by the circles. Chang et al. (2003a) also reported similar observation, where the aggregation of MMT was found at high MMT content (>5 wt%).

Figure 7 reports the FESEM micrographs of fractured cross-sectional surfaces of PLA/MMT/MCC hybrid composites and PLA/MMT/CNW hybrid nanocomposites, as reported in our previous studies (Arjmandi et al. 2015a, b). The fractured cross-sectional surfaces micrographs of P/MT5/MC1 hybrid composite, P/MT5/MC3 hybrid composite, P/MT5/CW1 hybrid nanocomposite and P/MT5/CW3 hybrid nanocomposite are presents in Fig. 7a–d, respectively. As can be observed from Fig. 7a, incorporation of MCC fillers (1 phr) into optimized PLA/MMT nanocomposites (P/MT5) led to aggregation of MCC in the PLA matrix, as indicated by the circle. This MCC aggregation likely resulted in the reduction of tensile strength compared to P/MT5 nanocomposite, as discussed earlier. As the concentration of MCC fillers increased in the hybrid composites, the aggregation of MCC was also increased (Fig. 7b), as indicated by the circle. Haafiz et al. (2013) and Mathew et al. (2005) were reported similar results, where MCC filled PLA composites using solution casting and melt mixing process, respectively.

In contrast, CNW disperses uniformly throughout the PLA/MMT nanocomposites; MMT fillers are indicated by the white arrows and the CNW particles by the red arrows (Fig. 7c). Accordingly, the interaction between the matrix and the

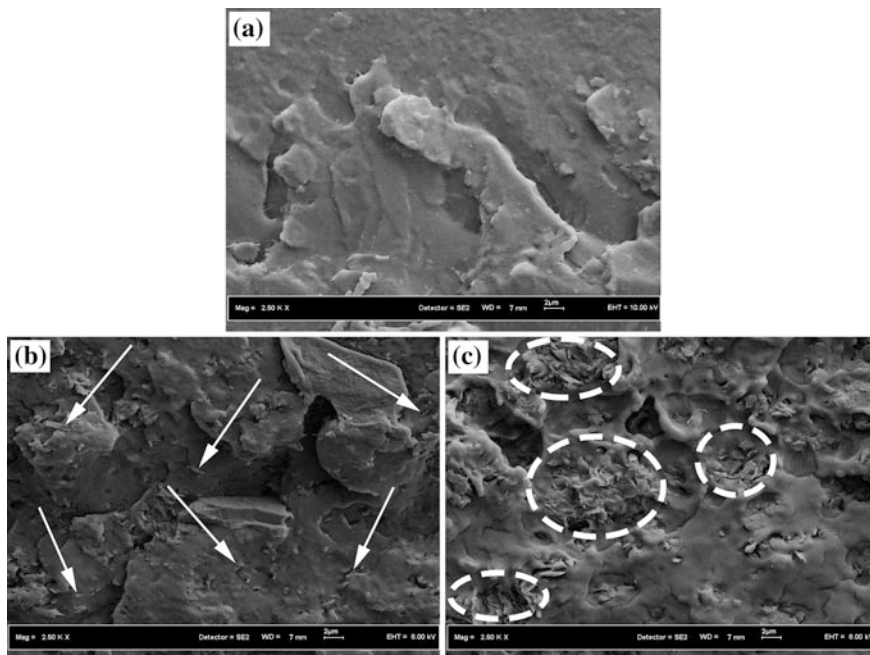


**Fig. 6** FESEM micrographs of fractured cross-sections of **a** neat PLA, **b** P/MT5 and **c** P/MT7 nanocomposites (Arjmandi et al. 2015a, b)

fillers has enhanced considerably, as reflected by an increased tensile strength. Meanwhile, at higher filler content filler-filler interactions are more favorable than filler-matrix interactions, leading to filler agglomeration. From Fig. 7d, agglomeration of the MMT filler (circled area) and the CNW particles (red arrows) in P/MT5/CW3 hybrid nanocomposite can be seen. This agglomeration plays a major role in decreasing the tensile properties of the PLA/MMT/CNW hybrid nanocomposites at high concentrations of CNW (>1 phr).

#### 4.5 Transmission Electron Microscopy

TEM micrographs of the neat PLA, P/MT5 nanocomposite, P/MT5/MC1 hybrid composite and P/MT5/CW1 hybrid nanocomposite have shown in Fig. 8a–d, respectively, as reported in our recent works (Arjmandi et al. 2015a, b). As can be observed from Fig. 8a, neat PLA clearly shows a smooth and clean surface with no obvious features. TEM micrograph of P/MT5 nanocomposite (Fig. 8b) shows that the MMT layers are intercalated in the PLA matrix, where the spaces between the dark lines are the interlayer spaces, as indicated by the white arrows. Similar observations were reported for PLA reinforced with MMT filler (Chang et al.



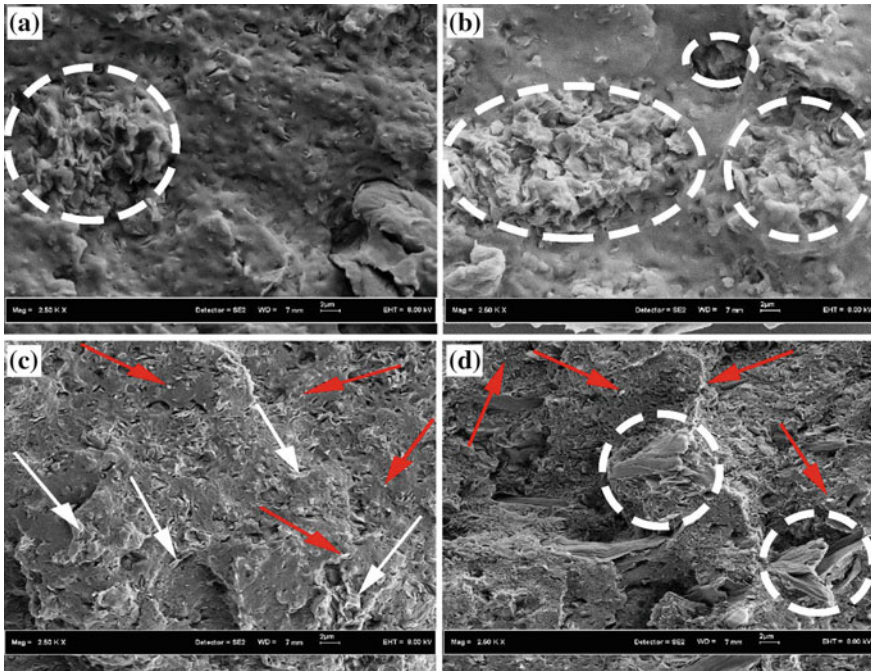


**Fig. 7** FESEM micrographs of fractured cross-sections of **a** P/MT5/MC1 hybrid composite **b** P/MT5/MC3 hybrid composite, **c** P/MT5/CW1 hybrid nanocomposite and **d** P/MT5/CW3 hybrid nanocomposite. MMT fillers are indicated by the *white arrow*, the CNW particles are indicated by a *red arrow* and the agglomerated MCC and MMT are indicated by *circles* (Arjmandi et al. 2015a, b)

2003a, b). The TEM micrograph of P/MT5 nanocomposite along with X-RD analysis (will be discussed in the next section) confirmed the formation of an intercalated structure system at 5 phr MMT content. TEM micrograph of P/MT5/MC1 hybrid composite (Fig. 8c) shows the aggregation of MCC particles (indicated by the circle) due to the unevenly dispersion and distribution of MCC fillers in the PLA matrix, where the MMT layers dispersed uniformly in the hybrid composite (indicated by the arrows). Cheng et al. (2012) reported similar observation for PLA/MMT/aluminum trihydrate hybrid composites. Besides that, the intercalation of MMT layers affected by aggregation of MCC particles, where the intercalation level reduced compared to P/MT5 nanocomposite.

However, as can be seen in Fig. 8d, the silicate-layered MMT evenly disperses throughout the PLA (white arrow), and most probably nanorod-like lines correspond to the CNW filler that uniformly disperses in the PLA matrix (red arrow). As can be observed from Fig. 8d, the CNWs stuck to the MMT and were also then covered by MMT platelets. Due to this, it is quite difficult to uniquely identify CNWs in the PLA/MMT/CNW hybrid nanocomposites. The good dispersion of MMT and CNW could be the reason for tensile strength improvements as

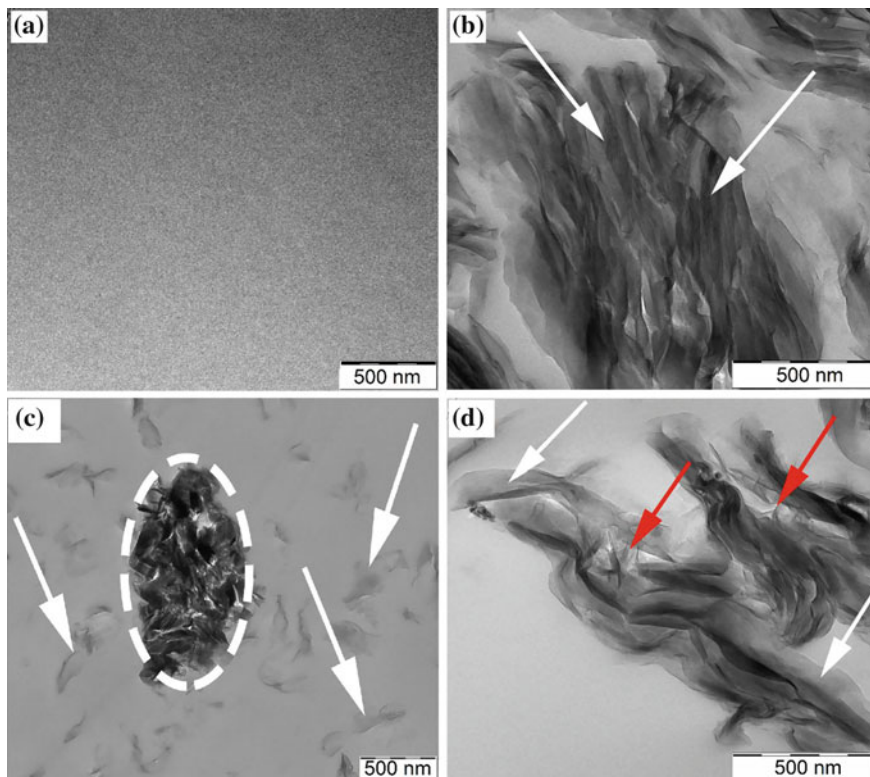


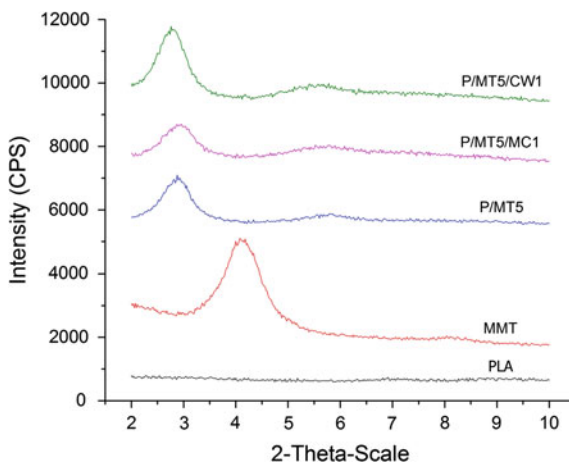
**Fig. 8** TEM micrographs of **a** neat PLA, **b** P/MT5 nanocomposite, **c** P/MT5/MC1 hybrid composite and **d** P/MT5/CW1 hybrid nanocomposite. MMT fillers are indicated by the *white arrows* and the CNW particles by the *red arrows* and the agglomerated MCC is indicated by a *circle* (Arjmandi et al. 2015a, b)

previously discussed. Additionally, it is speculated that given the evidence presented in Fig. 8d that the CNWs bind closely to the clay particles, increasing the available surface area for interaction with the PLA matrix. This effect could further enhance the stiffness of the nanocomposites. This finding indicates that the presence of a high content of CNW may induce the agglomeration of MMT filler and adversely affect the intercalation process of the MMT, leading to a decrease in the tensile strength.

#### 4.6 X-ray Diffraction Analysis

In order to further confirm the existence of the interaction between the fillers and the matrix, X-RD analysis of the nanocomposites was carried out. Figure 9 shows the X-RD patterns of the neat PLA and MMT, P/MT5 nanocomposite, P/MT5/MC1

**Fig. 9** X-RD pattern of neat PLA, neat MMT, P/MT5 nanocomposite, P/MT5/MC1 hybrid composite and P/MT5/CW1 hybrid nanocomposite (Arjmandi et al. 2015a, b)



hybrid composite and P/MT5/CW1 hybrid nanocomposite, as reported in our previous publications (Arjmandi et al. 2015a, b). Table 3 tabulates the relative  $d$ -spacing of the nanocomposites. The MMT filler exhibits a diffraction peak at  $2\theta = 4.15^\circ$ , corresponding to the 001 lattice plane which the  $d$ -spacing is dedicated to 2.14 nm. This peak shifts to a lower  $2\theta$  value as the MMT filler is incorporated into the PLA; the peak shifted to  $2\theta = 2.82^\circ$  which the  $d$ -spacing is dedicated to 3.15 nm. This result indicates that the scattering is due to an intercalation of the mineral phase by the PLA resin (Pettersson and Oksman 2006; Shyang and Kuen 2008). Moreover, this intercalation in the interlayer spacing of the MMT may be due to the formation of interactions with the PLA, thus providing the possibility for PLA chains to diffuse between the gallery layers of the MMT during processing (Balakrishnan et al. 2010). According to Balakrishnan et al. (2010), diffusion of PLA chains in the layers of MMT could increase the inter-gallery distance and also reduce the electrostatic attractions between abutting platelets. Besides that, the distribution of MMT layers in the PLA could be due to the intractions between ammonium groups of MMT and C=O groups of PLA chain segments which resulted in MMT intercalation. Other possible interactions between the PLA and the MMT filler may also occur via the -OH groups of the PLA and MMT (Jiang et al. 2007).

The  $d$ -spacing for the 001 peak of P/MT5/MC1 hybrid composite (Fig. 9) slightly decreased to 3.08 nm compared to optimized formulation of PLA/MMT

**Table 3** The  $2\theta$  angle and  $d$ -spacing of MMT, a P/M5 nanocomposite, a P/M5/C1 hybrid nanocomposite and a P/M5/C3 hybrid nanocomposite (Arjmandi et al. 2015a, b)

Sample	MMT	P/MT5	P/MT5/MC1	P/MT5/CW1
	001	001	001	001
$2\theta^\circ$	4.15	2.82	2.90	2.76
$d$ -spacing (nm)	2.14	3.15	3.08	3.21

nanocomposites (P/MT5) which dedicated to 3.15 nm, as summarized in Table 3. The decrease in  $d$ -spacing is confirmed the morphological properties which discussed earlier, where the incorporation of MCC into P/MT5 nanocomposite caused to aggregation of MCC, leading to fewer the intercalation of MMT in the hybrid nanocomposites. The effect of MCC agglomeration resulted in significant decrease in tensile strength compared to P/MT5 nanocomposite, although the decrease in  $d$ -spacing is small. However, incorporation of nano-size CNW into P/MT5 nanocomposite showed different behavior compared to micro-size MCC. The  $d$ -spacing for the 001 peak of P/MT5/CW1 hybrid nanocomposite (Fig. 9) slightly increased compared to P/MT5 nanocomposite (from 3.15 to 3.21 nm), as summarized in Table 3. This increase is an indication of a further enlarged interlayer space in the MMT nanostructure that could be due to the chain conformation of the matrix caused by a synergistic interaction with the CNW. In general, X-RD analysis of the PLA/MMT nanocomposites, PLA/MMT/MCC hybrid composites and PLA/MMT/CNW hybrid nanocomposites is well correlated with the tensile and morphological properties.

## 5 Conclusion and Future Perspective

Neat PLA, PLA/MMT nanocomposites, PLA/MMT/MCC hybrid composites and PLA/MMT/CNW hybrid nanocomposites were fabricated using solution casting method. Based on tensile strength, the optimum formulation of PLA/MMT nanocomposites was found at 5 phr MMT content. The Young's modulus of PLA/MMT nanocomposites, PLA/MMT/MCC hybrid composites and PLA/MMT/CNW hybrid nanocomposites increased gradually with increasing MMT, MCC and CNW content, respectively. The good dispersion and distribution of MMT fillers contributed to the enhanced tensile properties of PLA/MMT nanocomposites. Incorporation of MCC into P/MT5 nanocomposite led to aggregation of MCC in the hybrid composites. Due to the MCC aggregation in the hybrid composites, the  $d$ -spacing of MMT layers slightly decreased compared to P/MT5 nanocomposite, leading to less intercalation of MMT layers in the hybrid composites. It can be said that the incorporation of MCC into P/MT5 nanocomposite led to significant decrease in tensile strength, whereas the Young's modulus and ductility of hybrid composites increased significantly compared to P/MT5 nanocomposite. Nevertheless, the tensile strength of PLA/MMT/CNW hybrid nanocomposites increased significantly by incorporation of 1 phr CNW. Due to the possible nucleation of crazes in the amorphous fraction of the PLA and the formation of shear bands, the ductility of hybrid composites and hybrid nanocomposites increased significantly compared to PLA/MMT nanocomposites. The presence of polar interactions between the both fillers and PLA matrix were confirmed by FT-IR analysis. The formation of an intercalated nanostructure in PLA/MMT nanocomposites and PLA/MMT/CNW hybrid nanocomposites was confirmed by TEM and X-RD analysis. A uniform dispersion of CNW was readily apparent in the hybrid nanocomposites by incorporation of 1 phr CNW. Due to the presence of dispersed CNW in the

PLA/MMT/CNW hybrid nanocomposites, the interlayer spacing of the MMT slightly increased, leading to more intercalation, which in turn increased the tensile properties of the hybrid nanocomposites. The remaining challenge is to find an effective method to further enhance adhesion between PLA and both MMT and CNW. Overcoming this challenge is expected to further enhance the ductility, Young's modulus and tensile strength of these interesting materials.

**Acknowledgments** Authors wish to acknowledge the Universiti Teknologi Malaysia (UTM) and Research University Grant 05H22, sub-code: Q.J130000.2509.05H22 for financial support.

## References

- Arjmandi, R., Hassan, A., Haafiz, M.K.M., Zakaria, Z., Inuwa, I.M.: Characterization of polylactic acid/microcrystalline cellulose/montmorillonite hybrid composites. *Malays. J. Anal. Sci.* **18**, 642–650 (2014)
- Arjmandi, R., Hassan, A., Eichhorn, S.J., Haafiz, M.K.M., Zakaria, Z., Tanjung, F.A.: Enhanced ductility and tensile properties of hybrid montmorillonite/cellulose nanowhiskers reinforced polylactic acid nanocomposites. *J. Mater. Sci.* **50**, 3118–3130 (2015a)
- Arjmandi, R., Hassan, A., Haafiz, M.K.M., Zakaria, Z.: Effect of microcrystalline cellulose on biodegradability, tensile and morphological properties of montmorillonite reinforced polylactic acid nanocomposites. *Fiber Polym.* **16**, 2284–2293 (2015b)
- Azizi Samir, M.A.S., Alloin, F., Dufresne, A.: Review of recent research into cellulosic whiskers, their properties and their application in nanocomposite field. *Biomacromolecules* **6**, 612–626 (2005)
- Balakrishnan, H., Hassan, A., Wahit, M.U., Yussuf, A.A., Razak, S.B.A.: Novel toughened polylactic acid nanocomposite: mechanical, thermal and morphological properties. *Mater. Design* **31**, 3289–3298 (2010)
- Bulota, M., Hughes, M.: Toughening mechanisms in poly(lactic) acid reinforced with TEMPO-oxidized cellulose. *J. Mater. Sci.* **47**, 5517–5523 (2012)
- Chang, J.H., An, Y.U., Cho, D., Giannelis, E.P.: Poly(lactic acid) nanocomposites: comparison of their properties with montmorillonite and synthetic mica (II). *Polymer* **44**, 3715–3720 (2003a)
- Chang, J.H., An, Y.U., Sur, G.S.: Poly(lactic acid) Nanocomposites with Various Organoclays. I. Thermomechanical Properties, Morphology, and Gas Permeability. *J Polym Sci B* **41**, 94–103 (2003b)
- Chen, N.L., Feng, H.X., Guo, J.W., Luo, H.M., Qiu, J.H.: Biodegradable Poly(lactic acid)/TDI-montmorillonite nanocomposites: preparation and characterization. *Adv. Mat. Res.* **221**, 211–215 (2011a)
- Chen, W., Yu, H., Liu, Y., Chen, P., Zhang, M., Hai, Y.: Individualization of cellulose nanofibers from wood using high-intensity ultrasonication combined with chemical pretreatments. *Carbohydr. Polym.* **83**, 1804–1811 (2011b)
- Cheng, K.C., Yu, C.B., Guo, W., Wang, S.F., Chuang, T.H., Lin, Y.H.: Thermal properties and flammability of polylactide nanocomposites with aluminum trihydrate and organoclay. *Carbohydr. Polym.* **87**, 1119–1123 (2012)
- Cheng, Q., Wang, S., Rials, T.G.: Poly (vinyl alcohol) nanocomposites reinforced with cellulose fibrils isolated by high intensity ultrasonication. *Compos. Part A* **40**, 218–224 (2009)
- Cho, S.Y., Park, H.H., Yun, Y.S., Jin, H.J.: Cellulose nanowhisker-incorporated poly (lactic acid) composites for high thermal stability. *Fiber Polym.* **14**, 1001–1005 (2013)

- Chuayjuljit, S., Su-uthai, S., Charuchinda, S.: Poly(vinyl chloride) film filled with microcrystalline cellulose prepared from cotton fabric waste: properties and biodegradability study. *Waste Manag. Res.* **28**, 109–117 (2010)
- Field, L.D., Sternhell, S., Kalman, J.R.: *Organic structures from spectra*, 5th edn. Wiley, Chichester (2012)
- Haafiz, M.K.M., Hassan, A., Zakaria, Z., Inuwaa, I.M., Islam, M.S., Jawaid, M.: Properties of polylactic acid composites reinforced with oil palm biomass microcrystalline cellulose. *Carbohydr. Polym.* **98**, 139–145 (2013)
- He, Y.N., Guo, K., Chen, J.Z., Niu, M.J., Wang, W.J., Li, X.F.: Preparation and characterization of poly(lactic acid)/montmorillonite nanocomposites via a masterbatching method. *Adv. Mat. Res.* **335–336**, 1493–1498 (2011)
- Herrera, N., Mathew, A.P., Oksman, K.: Plasticized polylactic acid/cellulose nanocomposites prepared using melt-extrusion and liquid feeding: mechanical, thermal and optical properties. *Compos. Sci. Technol.* **106**, 149–155 (2015)
- Hong, J., Kim, D.S.: Preparation and physical properties of polylactide/cellulose nanowhisker/nanoclay composites. *Polym. Compos.* **34**, 293–298 (2013)
- Huda, M.S., Drzal, L.T., Mohanty, A.K., Misra, M.: Effect of fiber surface-treatments on the properties of laminated biocomposites from poly (lactic acid) (PLA) and kenaf fibers. *Compos. Sci. Technol.* **68**, 424–432 (2008)
- Iwatake, A., Nogi, M., Yano, H.: Cellulose nanofiber-reinforced polylactic acid. *Compos. Sci. Technol.* **68**, 2103–2106 (2008)
- Jiang, L., Zhang, J., Wolcott, M.P.: Comparison of polylactide/nanosized calcium carbonate and polylactide/montmorillonite composites: reinforcing effects and toughening mechanisms. *Polymer* **48**, 7632–7644 (2007)
- Karande, V.S., Bharimalla, A.K., Vigneshwaran, N., Kadam, P.G., Mhaske, S.T.: Cotton linter nano-fibers as the potential reinforcing agent for guar gum. *Iran. Polym. J.* **23**, 869–879 (2014)
- Lee, J., Sun, Q., Deng, Y.: Nanocomposites from regenerated cellulose and nanoclay. *J. Biobased Mater. Bio.* **2**, 162–168 (2008)
- Liu, M., Zhang, Y., Zhou, C.: Nanocomposites of halloysite and polylactide. *Appl. Clay Sci.* **75–76**, 52–59 (2013a)
- Liu, R., Luo, S., Cao, J., Peng, Y.: Characterization of organo-montmorillonite (OMMT) modified wood flour and properties of its composites with poly (lactic acid). *Compos. A* **51**, 33–42 (2013b)
- Lu, J., Wang, T., Drzal, L.T.: Preparation and properties of microfibrillated cellulose polyvinyl alcohol composite materials. *Compos. A* **39**, 738–746 (2008)
- Mathew, A.P., Oksman, K., Sain, M.: Mechanical properties of biodegradable composites from polylactic acid (PLA) and microcrystalline cellulose (MCC). *J. Appl. Polym. Sci.* **97**, 2014–2025 (2005)
- Oksman, K., Mathew, A.P., Bondeson, D., Kvien, I.: Manufacturing process of cellulose whiskers/polylactic acid nanocomposites. *Compos. Sci. Technol.* **66**, 2776–2784 (2006)
- Pandey, J.K., Chu, W.S., Kim, C.S., Lee, C.S., Ahn, S.H.M.: Bio-nano reinforcement of environmentally degradable polymer matrix by cellulose whiskers from grass. *Compos. B* **40**, 676–680 (2009)
- Pereda, M., Amica, G., Rácz, I., Marcovich, N.E.: Structure and properties of nanocomposite films based on sodium caseinate and nanocellulose fibers. *J. Food Eng.* **103**, 76–83 (2011)
- Petersson, L., Oksman, K.: Biopolymer based nanocomposites: comparing layered silicates and microcrystalline cellulose as nanoreinforcement. *Compos. Sci. Technol.* **66**, 2187–2196 (2006)
- Petersson, L., Kvien, I., Oksman, K.: Structure and thermal properties of poly (lactic acid)/cellulose whiskers nanocomposite materials. *Compos. Sci. Technol.* **67**, 2535–2544 (2007)
- Qu, P., Gao, Y., Wu, G., Zhang, L.: Nanocomposite of poly(lactid acid) reinforced with cellulose nanofibrils. *BioResources* **5**, 1811–1823 (2010)
- Sanchez-Garcia, M.D., Lagaron, J.M.: On the use of plant cellulose nanowhiskers to enhance the barrier properties of polylactic acid. *Cellulose* **17**, 987–1004 (2010)

- Satyamurthy, P., Jain, P., Balasubramanya, R.H., Vigneshwaran, N.: Preparation and characterization of cellulose nanowhiskers from cotton fibres by controlled microbial hydrolysis. *Carbohydr. Polym.* **83**, 122–129 (2011)
- Shayan, M., Azizi, H., Ghasemi, I., Karrabi, M.: Effect of modified starch and nanoclay particles on biodegradability and mechanical properties of cross-linked poly lactic acid. *Carbohydr. Polym.* **124**, 237–244 (2015)
- Shyang, C.W., Kuen, L.S.: Flexural, morphological and thermal properties of poly(lactic acid)/organo-montmorillonite nanocomposites. *Polym. Polym. Compos.* **16**, 263–270 (2008)
- Sinha Ray, S., Okamoto, M.: Polymer/layered silicate nanocomposites: a review from preparation to processing. *Prog. Polym. Sci.* **28**, 1539–1641 (2003)
- Thellen, C., Orroth, C., Froio, D., Ziegler, D., Lucciarini, J., Farrell, R., Ratto, J.A.: Influence of montmorillonite layered silicate on plasticized poly (L-lactide) blown films. *Polymer* **46**, 11716–11727 (2005)
- Vroman, I., Tighzert, L.: Biodegradable polymers. *Materials* **2**, 307–344 (2009)
- Wang, X., Qu, P., Zhang, L.: Thermal and structure properties of biobased cellulose nanowhiskers/poly (lactic acid) nanocomposites. *Fiber Polym.* **15**, 302–306 (2014)
- Wang, Y., Cao, X., Zhang, L.: Effects of cellulose whiskers on properties of soy protein thermoplastics. *Macromol. Biosci.* **6**, 524–531 (2006)